PASJ: Publ. Astron. Soc. Japan **65**, S13, 2013 December 5

Long-Period Oscillations of Sunspots by NoRH and SSRT Observations

Irina A. BAKUNINA,[1,2,3] Vladimir E. ABRAMOV-MAXIMOV,[3] Valery M. NAKARIAKOV,[4,3,5] Sergei V. LESOVOY,[6]
Alexander A. SOLOVIEV,[3] Yurii V. TIKHOMIROV,[2] Victor F. MELNIKOV,[3,2] Kiyoto SHIBASAKI,[7]
Yurii A. NAGOVITSYN,[3] and Elena L. AVERINA[1]

[1]*National Research University Higher School of Economics, 25/12 B. Pecherskaja ul., Nizhny Novgorod 603155, Russia*
rinbak@mail.ru

[2]*Radiophysical Research Institute (NIRFI), 25/12a, B. Pecherskaja ul., Nizhny Novgorod 603950, Russia*

[3]*Central Astronomical Observatory at Pulkovo, Russian Academy of Sciences, Pulkovskoe chaussee 65/1, St Petersburg 196140, Russia*
beam@gao.spb.ru

[4]*Physics Department, University of Warwick, Gibbet Hill Road, Coventry, CV4 7AL, UK*

[5]*School of Space Research, Kyung Hee University, Yongin, 446-701, Gyeonggi, Korea*

[6]*Institute of Solar-Terrestrial Physics, RAS SB, Lermontov St., 134, Irkutsk, 664033, Russia*

[7]*Nobeyama Solar Radio Observatory/NAOJ, 462-2 Nobeyama, Minamimaki, Minamisaku, Nagano 384-1305*
shibasaki@nro.nao.ac.jp

(Received 2013 April 1; accepted 2013 August 26)

Abstract

Long-term oscillations of microwave emission generated in sunspot magnetospheres are detected with the Nobeyama Radioheliograph (NoRH) at a frequency of 17 GHz, and the Siberian Solar Radio Telescope (SSRT) at 5.7 GHz. Significant periodicities in the range of 22–170 min are found in the variation of the emission intensity, polarisation and the degree of circular polarisation. Periods of the oscillations are not stable: they are different in different sunspots and in the same sunspot on different days. A cross-correlation analysis shows the presence of common significant periods in both NoRH and SSRT data. The cross-correlation coefficients are typically lower than 0.5, which can be attributed to the different heights of the emission formation, and different mechanisms for the emission generation (gyroresonance and thermal bremstrahlung at 17 GHz, and pure gyroresonance at 5.7 GHz). The observational results are consistent with the global sunspot oscillation model.

Key words: Sun: oscillations — Sun: radio radiation — Sun: sunspots

1. Introduction

Long-period oscillations, with the periods longer than 10 min, in the solar atmosphere attract attention because of several reasons. Interest in this kind of oscillations is connected with their possible link with helioseismological oscillations, the prominence formation and thermodynamics, and global oscillations of large scale structures, e.g., sunspots. Quasi-periodic oscillations of the integral solar radio flux at 3.3 cm, with characteristic periods of about 700 s (and also 250 s), were discovered three decades ago at the Zimenki Radioastronomical Station of NIRFI, Russia, by the group of M.M. Kobrin (Yudin 1968a, 1968b; Durasova et al. 1968). Periodic fluctuations of the solar radio flux were detected during both the growing phase of the solar activity and its minimum. It was suggested that the long-period oscillations were associated with either resonances in supergranules, or with global solar oscillations (Aleshin et al. 1973).

Analysis of the long-period oscillations in the solar radio emission required the development of dedicated techniques to account for the atmospheric artefacts and instrumental effects, which became possible only with the use of several independent radiotelescopes. In 1969 long-period fluctuations of the integral solar radio flux were studied at 4 cm with a small-base radiointerferometer at the Pulkovo Astronomical Observatory, Russia (Gelfreikh et al. 1969). The background noise was compensated by tuning the interferometer base, and its stability was carried out by the mechanical construction of the antenna system. Those experiments demonstrated that the integral solar radio flux almost always contains quasi-periodic fluctuations. Their amplitude and harmonicity were found to be highest during periods of high solar activity. A review of these pioneering studies of the quasi-periodic fluctuations in the solar integral radio flux was given in (Durasova et al. 1971).

Later, Kobrin et al. (1973) discovered quasi-periodic fluctuations of the integral solar radio flux at 3 cm with two 2-m parabolic antennae situated at Kislovodsk and Zimenki, about 1300 km apart. That experimental setup definitely ruled out an atmospheric origin of the periodicity, and confirmed that they are generated on the Sun. The detected periods included very long ones, up to two hours.

The long-period (longer than 30 min) quasi-periodic oscillations (LQPO) of sunspots are confidently detected in the optical band at the photospheric level (Nagovitsyn & Vyalshin 1990; Nagovitsyna & Nagovitsyn 2002; Efremov et al. 2007, 2008). The nature of sunspot LQPO is believed to be very different from the well-known 3 and 5-min oscillations. The latter are associated with standing and/or propagating MHD waves in the small magnetic flux tubes forming the sunspot, while the former are produced by the proper motion of a sunspot as a whole (Solov'ev & Kirichek 2008; Kshevetskii & Solov'ev 2008). Such oscillations can be possible if a sunspot is

a rather shallow object that protrudes into the convective zone of the Sun, as a column of strong magnetic field and cold plasma, up to depths of about few thousand kilometres only. This means that the magnetic flux tube of the sunspot expands sharply downward, starting with depths of about 4 Mm below the photosphere. The "shallow sunspot model," developed in (Solov'ev 1984a, 1984b; Solov'ev & Kirichek 2008, 2009; Kshevetskii & Solov'ev 2008), is consistent with an observational results obtained with local helioseismological techniques (Zhao et al. 2001; Zhao & Kosovichev 2004; Kosovichev 2006).

LQPO observed in sunspots as periodic Doppler shifts caused by vertical movements of plasmas, are seen to decrease rapidly with height (Efremov et al. 2007, 2008). Due to magnetic flux conservation and the frozen-in condition, these plasma movements are accompanied by variations in the magnetic field strength. The variation of the magnetic field over a sunspot causes a vertical displacement of the gyroresonance layer corresponding to a certain fixed observational wavelength. When this happens in a sharply stratified plasma of the chromosphere or the transition region, the radio flux generated at the gyroresonance layer obtains very pronounced modulation. Thus, there is an effect of amplification of the periodic signal of the sunspot oscillations observed in the radio band. Hence, radio LQPO can be observed (Gelfreikh et al. 2006) at heights well above the levels where both of the lines used in (Efremov et al. 2007, 2008) and photosphere continuum (Nagovitsyn & Vyalshin 1990; Nagovitsyna & Nagovitsyn 2002) are formed. A comparison of oscillatory processes at different heights of the solar atmosphere (Abramov-Maximov et al. 2007) using radio (Nobeyama Radioheliograph: NoRH, 17 GHz) and optical observations (the line-of-sight velocity in the line Fe 6495 Å) showed similar periodicities (80–100 min).

Radioheliographs with high spatial resolution have opened up new interesting perspectives in detailed studies of LQPO in sunspots. Recently, the LQPO in sunspots were studied with the NoRH (Gelfreikh et al. 2006; Abramov-Maximov et al. 2007; Bakunina et al. 2008; Chorley et al. 2010, 2011). It is also important to study LQPO observing them with two different, spatially separated instruments operating in the same band. The first attempt of such a study was carried out with the RT-7.5 radio-telescope (Moscow Region, Russia) at 93 GHz, and the RT-14 Metsähovi radio-telescope (Helsinki Region, Finland) at 37 GHz, and also with the 17 GHz data obtained with NoRH (Smirnova et al. 2011). Only two simultaneous sessions of observations, on 2010 July 1 and 2010 August 19, were analysed. Powerful, above the significance level of 95%, 16–60 and 80–130 min, and 10–50 and 60–130 min, LQPO were detected at 37 GHz and 93 GHz, simultaneously. In addition, a 70–130 min LQPO was seen at 17 GHz. A comparative analysis of 40–120 min LQPO in sunspots and related radio sources was recently carried out with the use of SOHO MDI and NoRH (Nagovitsyn et al. 2013). It was established that the LQPO periods of the radio sources are 12% longer. Phenomenological association of LQPO in a sunspot's chromosphere and in a diffuse fan-like EUV structure above it, observed with TRACE and NoRH, was established in (Yuan et al. 2011).

Very recently, a 200–400 min LQPO was found at 37 GHz with RT-14 (using the 9.5–11 hr time series) and in the line-of-sight component of the photospheric magnetic field, measured with the Helioseismic and Magnetic Imager instrument on-board the Solar Dynamics Observatory spacecraft (Smirnova et al. 2013b), see also (Smirnova et al. 2013a). A good correlation of the 37 GHz and the magnetic signals was established. The correlation coefficient was found to be 0.65, and even 0.72 if the magnetic field signal had a 15–18 min time lag. However, RT-14 and RT-7.5 have very limited spatial resolution, e.g., RT-14's beam size is 2′.4 at 37 GHz. A much better opportunity for the comparative study of LQPO observed at two spatially-separated locations is provided by the high spatial resolution radio facilities NoRH and the Siberian Solar Radio Telescope (SSRT) that both operate in the centimetre band. These instruments are situated about 1500 km apart, with a rather large observation time overlap of about 5 hr. The principles of image synthesis, implemented in these two instruments are different. NoRH is an aperture synthesis telescope, while the SSRT uses frequency scanning and the rotation of the Earth. Thus, the simultaneous detection of LQPO with these instruments excludes completely both atmospheric and instrumental origins of the periodicity. However, full exploitation of the advantages of the high spatial resolution provided by the radioheliographs requires development of dedicated data analysis techniques. These techniques should take into account the complexity of both the investigated physical phenomena and the instruments (e.g., Sych & Nakariakov 2008).

The aim of this paper is to study LQPO of the microwave emission originating over sunspots, with the simultaneous use of two different instruments, NoRH and SSRT, and to assess the statistical significance of these oscillations.

2. Data

For the analysis of LQPO we choose seven large sunspots in the active regions AR 9463, 10008, 10296, 10673, 10743, 10904, and 10963. The sunspots had bipolar (AR 9463, 10008, 10296, 10673, 10904, 10963) or unipolar (AR 10743) configurations of the magnetic field. The diameters of the analysed sunspots were greater than 0′.7. The microwave sources over these sunspots did not show any evident flaring activity during the period of observations. We used time sequences of high spatial resolution microwave images obtained with two different instruments, the Nobeyama Radioheliograph (NoRH, the frequency 17 GHz, spatial resolution 10″) and the Siberian Solar Radio Telescope (SSRT, the frequency 5.7 GHz, spatial resolution 20″). The observational times of these instruments overlap by approximately 5 hr. In addition, SOHO/MDI data were used for sunspot selection and the identification of their magnetic configuration.

2.1. NoRH Data

Time series of the 17 GHz signals measured by NoRH, were obtained from sequences of synthesised full-Sun microwave images with a cadence time of one minute and integration time of 10 s. In each image the microwave source was associated with a certain sunspot. Then, a region-of-interest was selected around the microwave source (taking into account the solar

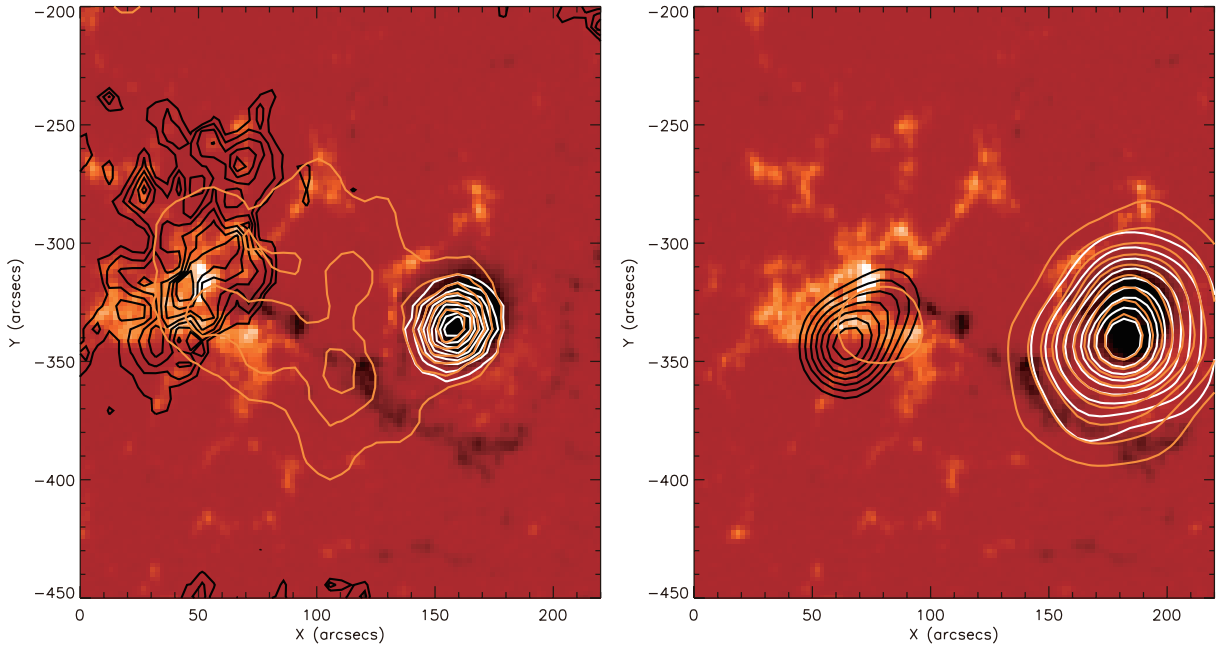

Fig. 1. MDI magnetogram of AR 10673 on 2004 September 22. The white colour corresponds to the negative magnetic polarity. The yellow contours show the microwave intensity, and the black (white) contours show the degree of right- (left-) hand circular polarisation at the levels 0.1, 0.3, 0.5, 0.7, 0.9. Panel (a) shows the results obtained with NoRH at the 17 GHz at time 02:44:36 UT; panel (b) shows the SSRT results at 5.7 GHz at time 05:08:29 UT.

rotation). In the microwave sources, the maxima of the radio brightness temperatures, $T_{\rm b}^{\rm (I)}$ and $T_{\rm b}^{\rm (V)}$, obtained for the intensity, I, and the polarisation, V, respectively, were determined.

In quiescent sunspots the time evolution of the integral brightness temperature practically coincides with the time evolution of the maximum brightness temperature. Thus, in our study it would be sufficient to consider only the time variation of the maximum temperature. However, a more reliable approach is to use the average value of the brightness temperature over the sunspot area. This method eliminates the effects of the diurnal variation of the instrumental spatial resolution. Thus, in our study we use both of these quantities: the maximum brightness temperature found in the 16 × 16-pixel box around the radio source (1 pixel equals about 5″), and the value of brightness temperatures of the intensity, I, and the polarisation, V, averaged over this box 10 × 10 pixels, centred at the maximum brightness. The data stationarisation is discussed in subsection 2.4.

2.2. *SSRT Data*

The time series of the 5.7 GHz signals obtained with SSRT are the time evolution of the brightness temperature of a chosen target sunspot, averaged over an area of about 25″ × 25″. The cadence is one minute and the signal integration time is 0.3 s. Since the SSRT data have a variable sampling time that varies in the range 0.5–2 min, the constant cadence was obtained by interpolation.

The absolute value of the brightness temperature was determined by the signals of the quiet Sun and the sky. At the same instant of time, an arbitrary chosen image of the full disk was calibrated, and then the average brightness temperature of a microwave source of interest was obtained. This value sets up the reference level for the calibration of the time series. It is important to take into account both the quite Sun and the sky emission fluxes in the calibration, as the calibration that is based upon the solar signal only gives a daily trend caused by the stronger change of the signal from the extended full-disk source in comparison with the compact source associated with the sunspot. The data stationarisation is discussed in subsection 2.4.

2.3. *Circular Polarisation*

As at 17 GHz, the gyro-resonance emission is generated at the third harmonics of the electron gyro-frequency, corresponding to the absolute value of a magnetic field of about 2000 G, the degree of circular polarisation of the emission from a large sunspot should be about 100%. However, in our observations the degree of circular polarisation was in the range of 50%–90%. This is likely to be connected with the presence of a source of thermal bremsstrahlung emission together with the gyroresonance source over the sunspot (see figure 1a). In contrast to the 17 GHz channel, at 5.7 GHz the effect of the thermal emission is seen to be negligible (figure 1b). Hence, the compared signals can differ from each other quite significantly.

Because of the instrumental amplitude-frequency non-stationarity of SSRT, the most suitable variable for this study is the degree of circular polarisation, $\mathcal{P}_{\rm SSRT}$. It is calculated as the time evolution of the ratio of the brightness temperatures measured in the intensity and polarisation channels, averaged over an area of about 25″ × 25″, of the target sunspot. Normally, the effect of the non-stationarity on the signal in the I and V channels is practically identical, and hence cancels out.

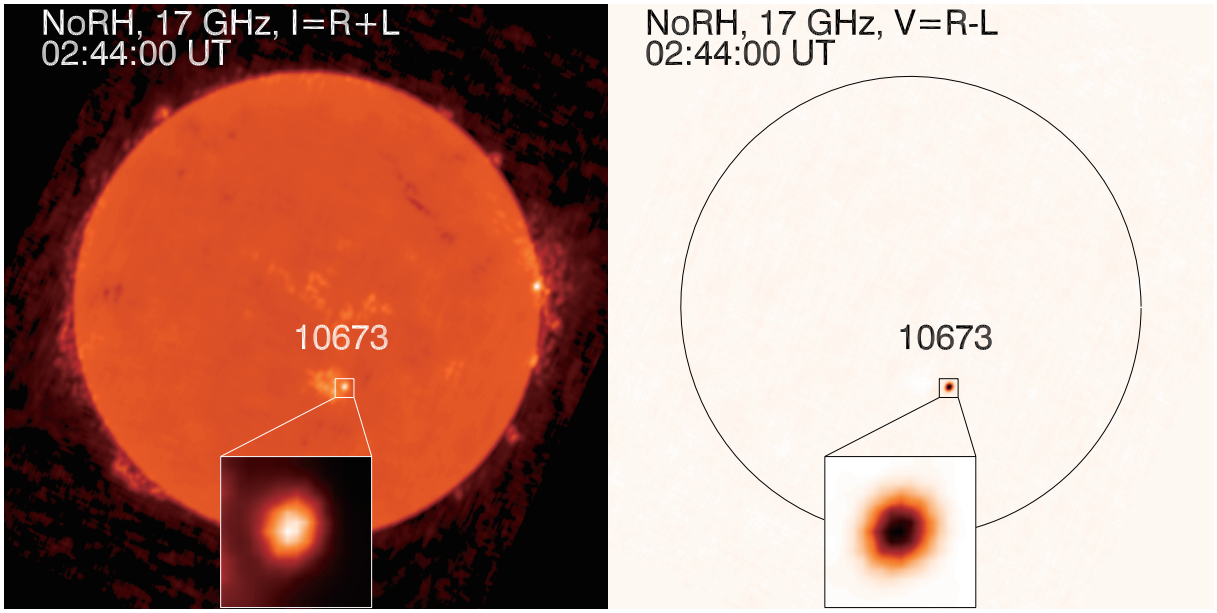

Fig. 2. Leading sunspot of AR 10673 on 2004 September 22 inside the box 16 × 16 pixels.

In the case of NoRH data, the degree of polarisation can be defined either as $\mathcal{P}_{\max} = \max(T_{\rm b}^{(\rm V)})/\max(T_{\rm b}^{(\rm I)})$ for the maximum brightnesses, or $\mathcal{P}_{\rm aver} = \langle T_{\rm b}^{(\rm V)}\rangle/\langle T_{\rm b}^{(\rm I)}\rangle$ for the average brightnesses. Averaging is performed over a box of $50'' \times 50''$, (see figure 2) over the target sunspot. In the statistical analysis (table 4) we used both signals, $\mathcal{P}_{\max}$ and $\mathcal{P}_{\rm aver}$.

2.4. *Data De-Trending*

The daily variation of the signal, connected with the variation of the area of the radio interferometers due to the movement of the Sun over the sky, was removed by subtracting a polynomial. The choice of the degree of the approximating polynomial was based upon the following technique. For the initially non-stationary series, for different degrees of the polynomial p, we calculated the differences $\Delta_t^{(1)} = y_t - y_{t-1}$, $\Delta_t^{(2)} = \Delta_t - \Delta_{t-1}$, etc., until the autocorrelation function,

$$\hat{\rho_k} = \frac{\Sigma_{t=k+1}^{n}(\Delta_t^{(p)} - \langle\Delta_t^{(p)}\rangle)(\Delta_{t-k}^{(p)} - \langle\Delta_t^{(p)}\rangle)}{\Sigma_{t=1}^{n}(\Delta_t^{(p)} - \langle\Delta_t^{(p)}\rangle)^2}, \qquad (1)$$

where $k = 1, 2, \cdots$ did not decline quickly enough with the growth of k (starting with $k = p + 1$), which indicated the stationarity of the series. This procedure determines the power, p, of the approximating polynomial. In the majority of analysed cases, the suitable order of the trend-approximating polynomial, $P_t^{(4)}$, was found to be four.

Another source of non-stationarity of the analysed signals is the ionospheric variations and transient processes on the Sun. We suppress these effects in the data by smoothing the signal by nine minutes. Then, the data series were detrended for statistical analysis (see table 4) by centring them to a zero mean,

$$y_n = (y_t - P_t^{(4)})/P_t^{(4)}, \qquad (2)$$

where y_t is the current element of the series, and $P_t^{(4)}$ is the current value of the polynomial trend. The detrended and centred datasets were analysed using a Fourier (e.g., the Scargle periodogram: Scargle 1982) and wavelet techniques (Torrence & Compo 1998; Torrence & Webster 1999), and autocorrelation and cross-correlation methods.

2.5. *Cross-Correlation of the Time Series Obtained by Image Synthesis and Average Correlation Amplitude Time Profiles Obtained with NoRH at 17 GHz*

The first question is whether the analysed signal is of solar origin. To answer this question, we used time profiles of the long-base average correlation amplitude of NoRH (NoRH correlation plots). The correlation plots were obtained by averaging the correlation coefficients of those antenna pairs that are separated by distances greater than $100\,s_0$, where s_0 is 1.528 m. Those pairs "see" only small-scale sources on the solar disk, smaller than $24''$ in the zenith. All larger sources that correspond to the quiet Sun emission, the Earth's atmospheric effects, and the side lobes of the antenna functions, are filtered out by this approach. The cross-correlation of the time profiles of the long-base average correlation amplitude with the time evolution of the maximum and average brightness temperatures over a sunspot was calculated. This allows one to detect the time variability that is intrinsic to the sunspot, but only in the case when there are no other significant sources on the solar disk. The sensitivity of the correlation plots is known to have a higher signal-to-noise ratio than the signals obtained from the sequences of synthesised images, since the lower spatial harmonics present in the full disk images contain the full disk noise (Nakajima et al. 1994). Because the exact u–v plane[1] coverage changes during the day, and this affects the measurements, comparing time curves obtained using all baselines with the time curves obtained without the short

[1] The u–v plane is a Fourier-transform of the angular radio brightness distribution over the emission source.

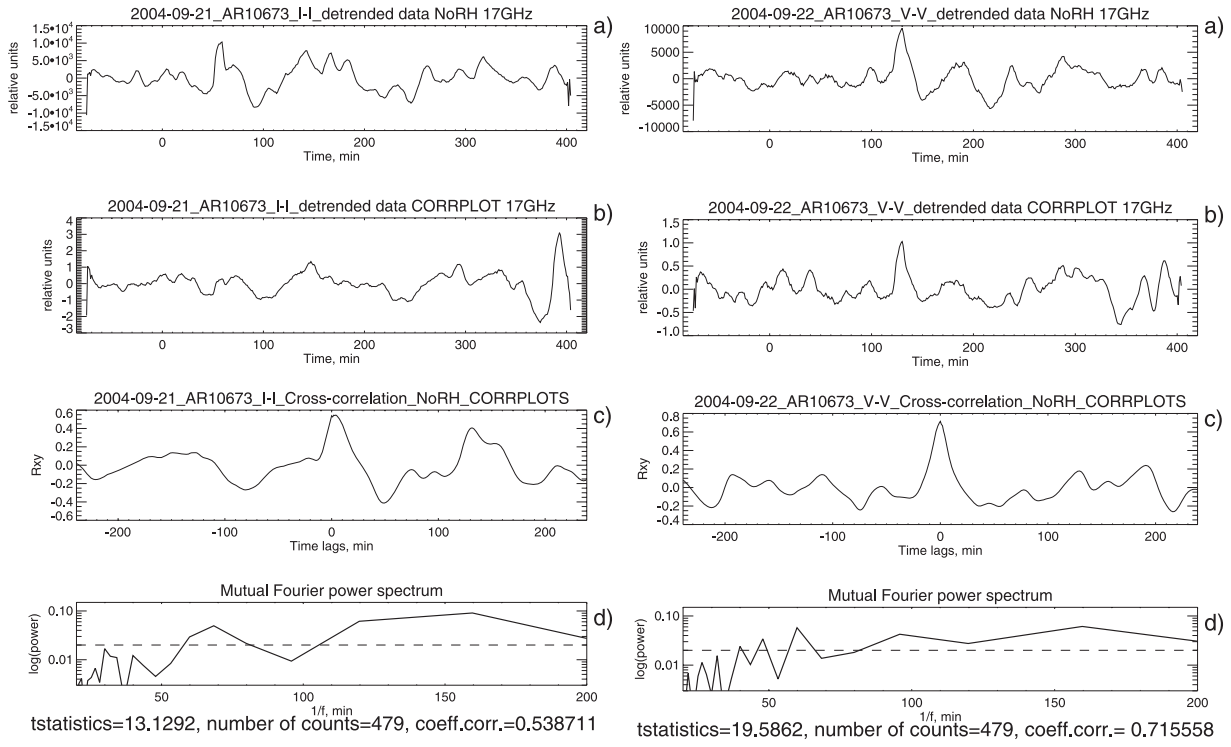

Fig. 3. Analysis of the intensity signal (left column) of the radio source above the leading sunspot in AR 10673 on 2004 September 21, and polarisation signal (right column) of the radio source above the leading sunspot in AR 10673 on 2004 September 22, measured with NoRH at 17 GHz. Panel (a): Time profiles obtained by image synthesis. Panel (b): Time profiles of the long-base average correlation amplitude (NoRH correlation plots). Panel (c): Cross-correlation functions of the signals shown in panels (a) and (b). Panel (d): Mutual Fourier spectra [the Fourier power spectra of the cross-correlation functions shown in panel (c)].

baselines can be considered as a proof of solar, not instrumental origin of the fluctuations.

Consider the microwave emission coming from the leading sunspot of AR 10673 for two days, 2004 September 21 and 22 (see figure 3). The figures reveal that the signals obtained by image synthesis and by long-base average correlation show good cross-correlation in both the intensity and polarisation. Specifically, the cross-correlation coefficient of the intensity signals on 2004 September 21 is 0.54, and 0.72 on 2004 September 22. Moreover the Student's t-coefficients are found to be 13.13 and 19.59, which is significantly higher than 3.41. The student's t-test for statistical significance of a cross-correlation coefficient is used for comparing two independent sets of data with similar standard deviations (Walpole et al. 2002). In particular, samples with the number of data points greater than 100 are taken to correlate with each other with a 5% confidence interval (95% probability) if the value of the Student t-coefficient exceeds 3.41 (Fuller 1976). This demonstrates the solar origin of the analysed variability. The cross-correlation functions, which are the dependence of the cross-correlation coefficient on the time lag between the two compared signals, have significant LQPO with the periods of about 70 and 150 min on 2004 September 21, and 60 and 130 min on 2004 September 22. These peaks are well seen in the mutual Fourier power spectra that are the Fourier power spectra of the cross-correlation functions. According to the discussion above, these LQPO are of solar origin.

Figure 4 shows the same analysis applied to the NoRH data obtained on 2004 September 23 in both intensity and polarisation channels. The cross-correlation coefficients are not very high (0.44 in intensity and 0.52 in polarisation) as obtained for 2004 September 21 and 22, while the Student's t-coefficients are sufficiently high (10.26 and 13.51, respectively). The cross-correlation functions also show a pronounced LQPO. The periods are 50, 70, and 120 min in intensity, and 55, 70, and 120 min in polarisation.

2.6. *Comparative Analysis of the Time Profiles Obtained with NoRH and SSRT*

The time dependences of the microwave intensity, polarisation and degree of polarisation recorded with NoRH and SSRT were compared using two different methods:

(1) *Calculation of the cross-correlation function of the detrended signals (see subsection 2.4) obtained with these instruments.* The function is the dependence of the cross-correlation coefficient of the signals on the time lag between the signals. We then estimated the statistical significance of the highest value of the correlation coefficient, and constructed the Fourier power spectrum of the cross-correlation function (the mutual Fourier spectrum). The statistical significance of spectral peaks was estimated according to Scargle (1982).

(2) *Construction of wavelet spectra of the autocorrelation functions of signals obtained with different instruments, and their comparison with the mutual Fourier spectra.* This approach is rigorous because of the absence of a theorem similar to the Wiener–Khinchin theorem for the wavelet

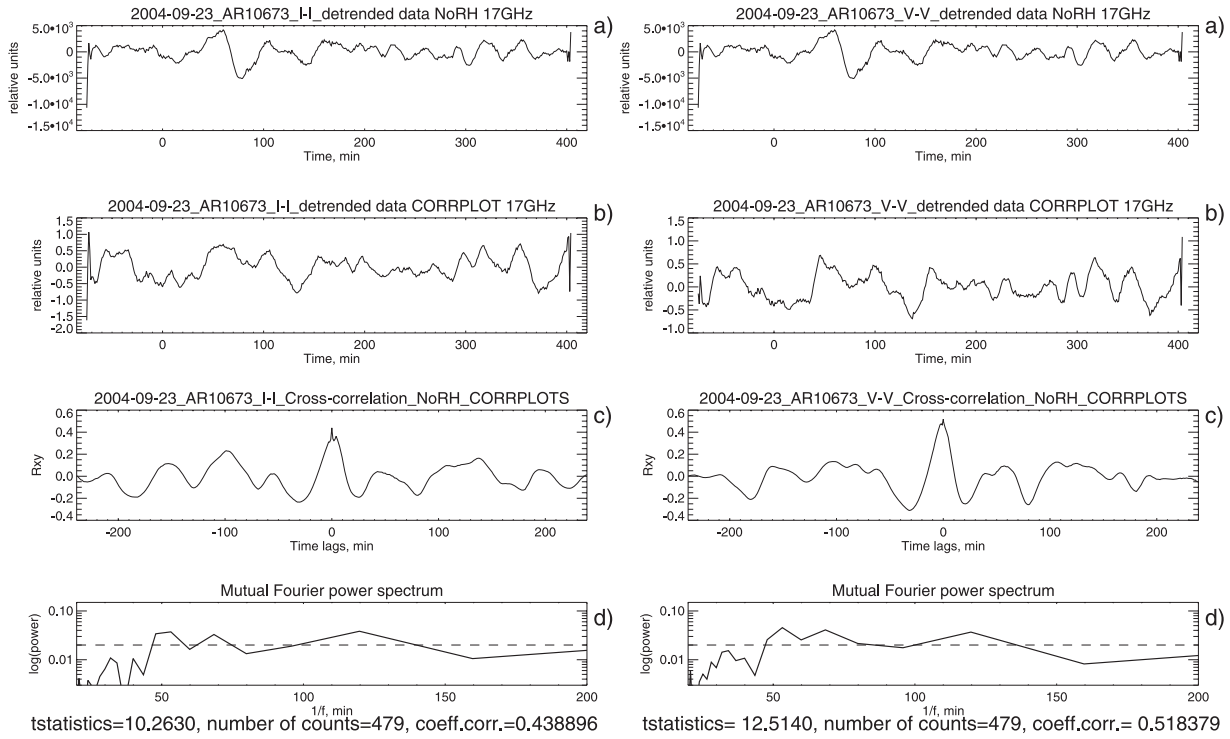

Fig. 4. Same as in figure 3, but for the intensity (left column) and polarisation (right column) signals of the radio source above the leading sunspot in AR 10673 on 2004 September 23.

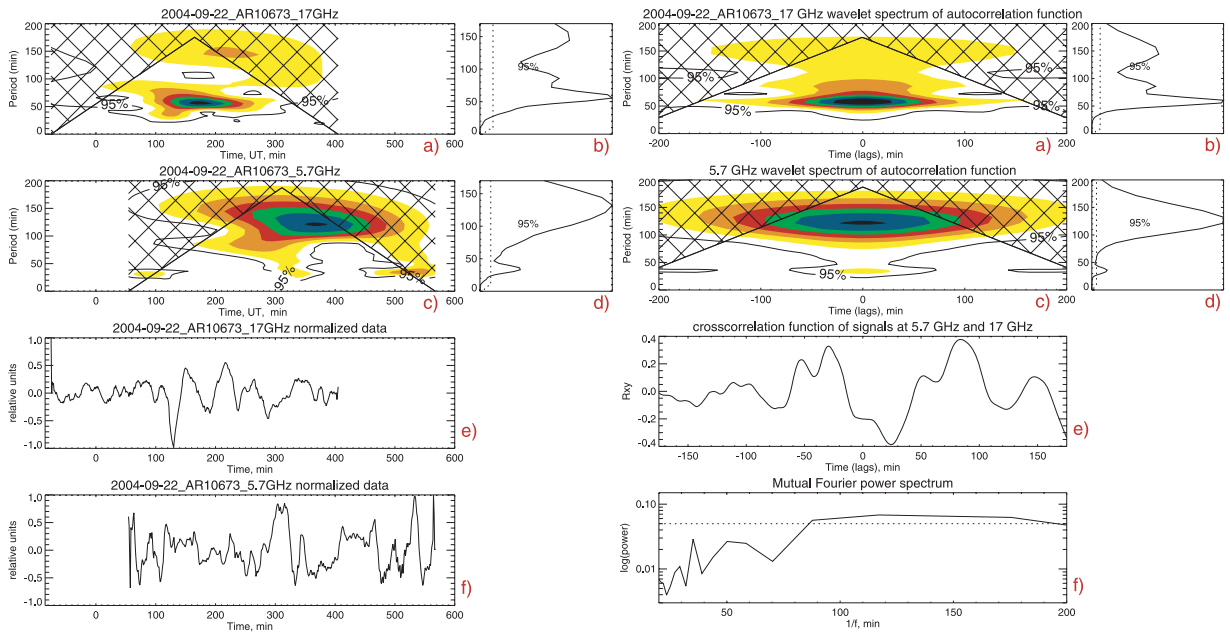

Fig. 5. Cross-correlation analysis of the radio brightness temperature, $T_b^{(I)}$, of the radio source above the leading sunspot in AR 10673 on 2004 September 22. Left column: Wavelet spectra of the signals at 17 GHz by NoRH and 5.7 GHz by SSRT [panels (a) and (c), respectively]; global wavelet spectra of those signals [(b) and (d), respectively]; detrended and centred signals $T_b^{(I)}$ obtained by NoRH at 17 GHz and SSRT at 5.7 GHz [(e) and (f), respectively]. Right column: Wavelet spectra of the autocorrelation functions of the parameter $T_b^{(I)}$ at 17 and 5.7 GHz frequencies [(a) and (c), respectively], their global wavelet spectra [(b) and (d), respectively], the cross-correlation function of the signals (e), and its Fourier spectrum (f). Statistical properties of the cross-correlation are shown in table 1.

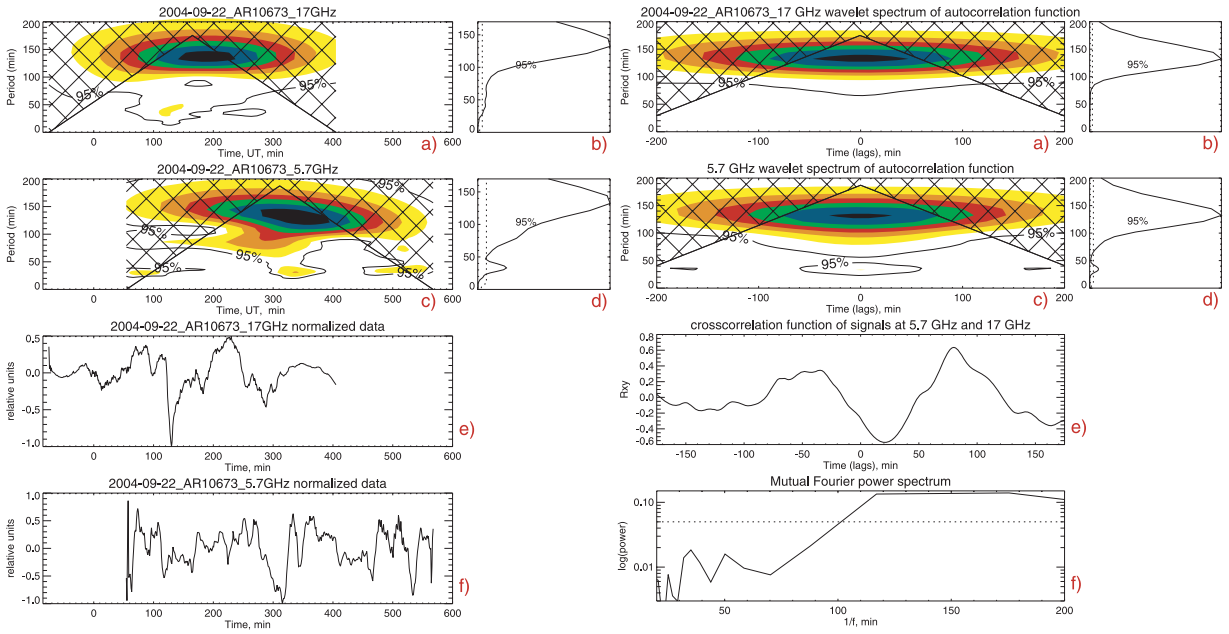

Fig. 6. Same as in figure 5, but for $T_{\rm b}^{\rm (V)}$. These statistical properties of the cross-correlation are given in table 2.

Table 1. Correlation of time profiles of the radio brightness temperatures, $T_{\rm b}^{\rm (I)}$.*

	t (Student's t-coefficient)	r (cross-correlation coefficient)	n (number of counts)	T (common periods, min)
Time profiles	3.79	−0.20	351	130
Auto-correlation functions	2.57	0.17	239	130

* Obtained at 17 GHz and 5.7 GHz with NoRH and SSRT, respectively, in the intensity channel, and their auto-correlation functions, for AR 10673, 2004 September 22, (see figure 5).

Table 2. Correlation of the time profiles of the radio brightness temperatures, $T_{\rm b}^{\rm (V)}$.

	t (Student's t-coefficient)	r (cross-correlation coefficient)	n (number of counts)	T (common periods, min)
Time profiles	5.09	−0.27	351	130
Auto-correlation functions	8.66	0.51	239	130

* Obtained at 17 GHz and 5.7 GHz with NoRH and SSRT, respectively, in the polarisation channels, and their auto-correlation functions, for AR 10673, 2004 September 22, (see figure 6).

spectrum of an autocorrelation function, and a lack of understanding of the physical meaning of the wavelet spectrum of the autocorrelation function. However, qualitatively, the results obtained with this approach are consistent with those obtained using the cross-correlation function. The advantages of the wavelet approach are the possibility to study the time evolution of the period of interest. The statistical significance was estimated according to the χ^2-criterion (Torrence & Compo 1998).

Figures 5 and 6 show that the cross-correlation functions have a common period of oscillation, about 130 min, in both the intensity and polarisation channels. The correlation of the signals obtained by SSRT and NoRH are given in tables 1 and 2. In the polarisation, the correlation coefficient is about 0.27 with a t-coefficient of about 5.09. In the intensity the correlation is worse; the correlation coefficient is −0.20 with a t-coefficient of 2.57. However, since the same period was also found in the correlation plots in the polarisation channel, we conclude that this periodicity is of solar origin.

Figure 7 and table 3 show another example, for the time dependence of the degree of circular polarisation, $\mathcal{P}_{\rm max}$, recorded with SSRT and NoRH on 2007 April 28 over AR 10953. The time series have the correlation coefficient of −0.38 and t-coefficient 5.2. In this case, both SSRT and NoRH data have significant LQPO with a period of 83 min.

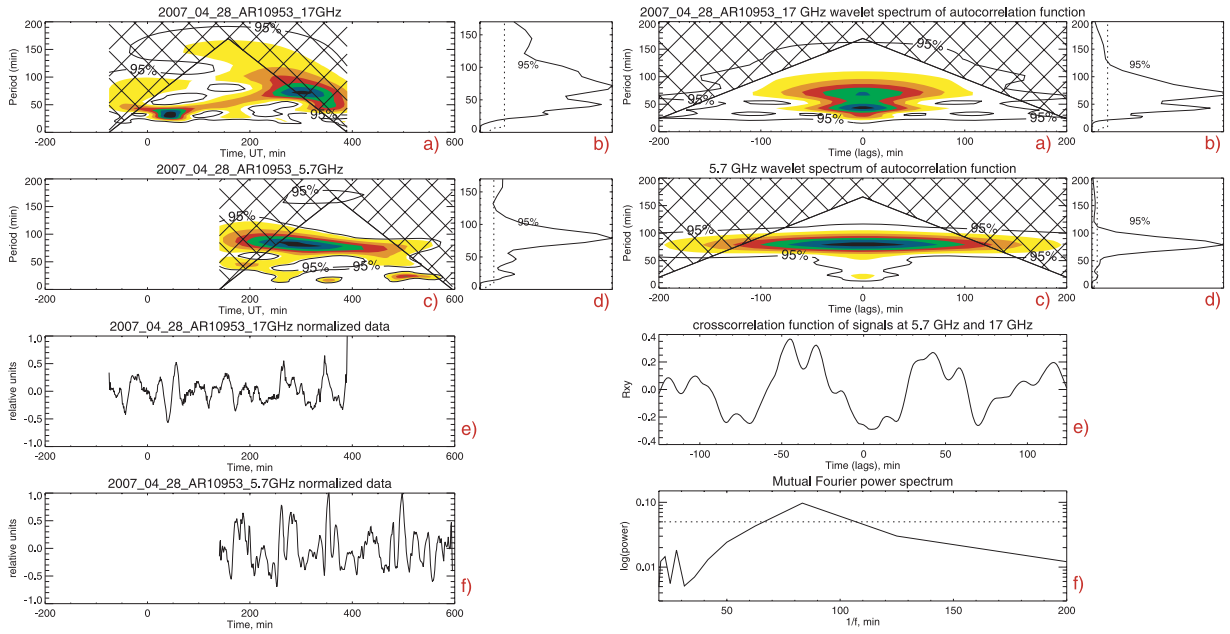

Fig. 7. Same as in figure 5, but for the degree of circular polarisation, $\mathcal{P}_{\max}$, for AR 10953, 2007 April 28. Statistical properties of the cross-correlation are given in table 3.

Table 3. Correlation of the degree of circular polarisation $\mathcal{P}_{\max}$.

	t (Student's t-coefficient)	r (cross-correlation coefficient)	n (number of counts)	T (common periods, min)
Time profiles	4.07	−0.26	250	40, 83
Auto-correlation functions	8.72	0.52	232	83

* Obtained at 17 GHz and 5.7 GHz with NoRH and SSRT, respectively, and their auto-correlation functions, for AR 10953, 2007 April 28 (see figure 7).

The results of a correlation analysis performed for seven large sunspots and fifteen days of observations, are summarised in table 4. Here, we present the cross-correlation and Student's t-coefficients calculated for the signals obtained with SSRT at 5.7 GHz and NoRH AT 17 GHz. As discussed in subsections 2.1–2.3, two kinds of NoRH signals were used: the time variation of the maximum brightness temperature of the radio source, and the value of the brightness temperatures averaged over a 10 × 10-pixel box that included the radio source. Also, table 4 gives the common periods found by cross-Fourier periodogram analysis. The significance (99%) was estimated according to Scargle (1982). In addition, we give the maximum absolute values of the degree of circular polarisation for all three kinds of data used in this study.

3. Discussion and Conclusions

We performed an analysis of LQPO in the microwave emission generated at different sunspots, detected by different techniques with the use of different, spatially separated instruments, SSRT and NoRH. The simultaneous presence of LQPO in the SSRT and NoRH data confirms the solar origin of the oscillations. Some analysed datasets revealed a significant (while rather weak) correlation between the various parameters of the radio emission recorded with SSRT and NoRH: the intensity, polarisation and degree of circular polarisation.

The obtained results can be summarised as follows:

1. LQPO in the microwave sources over sunspots with periods longer than 30 min were confidently detected by both NoRH and SSRT, and found to have periods similar to those found in previous optical and radio observations.

2. The solar origin of LQPO in the NoRH data was proven by the method of the cross-correlation of time profiles of brightness temperatures obtained from images of solar active regions, and the correlation amplitudes (temporal profiles derived from multiplying the signals from pairs of remote antennae of the interferometer).

3. Significant LQPO with periods 30–170 min were found in both SSRT (5.7 GHz) and NoRH (17 GHz) data for seven sunspots in fifteen days of observations.

4. Periods of LQPO are found to be not stable at both observational frequencies. The periods are different in different sunspots. In the same sunspot, LQPO can have different periods on different days. Also, different physical parameters

Table 4. Results of the analysis.*

No	Object	Signals	n	t_1	t_2	r_1	r_2	P_1	P_2
1	10008	I	372	1.9	4.6	−0.1	−0.23	55, 75, 125	55, 75, 125
	24.06.2002	V	372	3.55	1.46	0.18	0.08	35, 55, 75, 125	75, 180
	$\mathcal{P}^{\max}_{\max} = -90\%$	$\mathcal{P}$	372	6.02	2.32	−0.31	0.12	35, 65, 125	35, 75, 125
	$\mathcal{P}^{\max}_{\text{aver}} = -70\%$								
	$\mathcal{P}^{\max}_{\text{SSRT}} = -7\%$								
2	10296	I	259	4.66	4.40	0.28	0.27	45, 130	45, 130
	04.03.2003	V	259	2.4	0.93	0.15	0.06	35, 130	35, 65–130
	$\mathcal{P}^{\max}_{\max} = 60\%$	$\mathcal{P}$	259	1.66	4.03	−0.10	−0.25	30, 85, 130	35, 65, 130
	$\mathcal{P}^{\max}_{\text{aver}} = 55\%$								
	$\mathcal{P}^{\max}_{\text{SSRT}} = 13\%$								
3	10296	I	303	0.52	1.08	0.03	0.06	45, 60, 100, 150	60, 150
	06.03.2003	V	303	0.02	0.44	0.00	0.03	43, 60, 100	65, 90, 150
	$\mathcal{P}^{\max}_{\max} = 85\%$	$\mathcal{P}$	303	3.03	0.74	0.04	0.17	45, 100, 155	30, 150
	$\mathcal{P}^{\max}_{\text{aver}} = 70\%$								
	$\mathcal{P}^{\max}_{\text{SSRT}} = 15\%$								
4	10296	I	311	2.28	1.57	0.13	0.09	45, 62, 155	45, 62, 155
	08.03.2003	V	311	2.01	1.76	0.11	0.1	45, 155	45, 80, 155
	$\mathcal{P}^{\max}_{\max} = 77\%$	$\mathcal{P}$	311	5.75	5.97	0.32	0.33	32, 62, 155	62, 155
	$\mathcal{P}^{\max}_{\text{aver}} = 65\%$								
	$\mathcal{P}^{\max}_{\text{SSRT}} = 18\%$								
5	10306	I	226	0.05	0.51	−0.003	−0.03	35, 110	35, 75, 150
	11.03.2003	V	226	1.41	1.43	−0.09	−0.1	35, 75	35, 75, 110
	$\mathcal{P}^{\max}_{\max} = 67\%$	$\mathcal{P}$	226	5.53	2.21	0.36	0.15	35, 110	32, 75, 110
	$\mathcal{P}^{\max}_{\text{aver}} = 65\%$								
	$\mathcal{P}^{\max}_{\text{SSRT}} = 12\%$								
6	10306	I	306	1.29	1.16	0.07	−0.07	45, 75, 155	38, 75, 155
	12.03.2003	V	306	2.93	2.45	−0.17	−0.14	38, 75, 155	38, 75, 155
	$\mathcal{P}^{\max}_{\max} = 87\%$	$\mathcal{P}$	306	0.04	0.24	−0.002	0.01	25, 35, 45, 100	25, 40, 100
	$\mathcal{P}^{\max}_{\text{aver}} = 80\%$								
	$\mathcal{P}^{\max}_{\text{SSRT}} = 13\%$								
7	10306	I	264	6.58	6.46	0.39	0.38	38, 85, 145	30, 38, 85–140
	13.03.2003	V	264	6.70	5.3	0.39	0.32	85, 140	30, 38, 85, 140
	$\mathcal{P}^{\max}_{\max} = 92\%$	P	264	1.2	2.5	0.08	0.16	25, 90	90
	$\mathcal{P}^{\max}_{\text{aver}} = 80\%$								
	$\mathcal{P}^{\max}_{\text{SSRT}} = 13\%$								
8	10673	I	348	5.39	1.78	0.28	0.1	90, 175	45, 85, 175
	21.09.2004	V	348	3.85	5.41	0.20	0.28	58, 88–175	58, 175
	$\mathcal{P}^{\max}_{\max} = -72\%$	$\mathcal{P}$	348	0.018	0.39	0.00	0.02	38, 58, 88, 180	58, 175
	$\mathcal{P}^{\max}_{\text{aver}} = -34\%$								
	$\mathcal{P}^{\max}_{\text{SSRT}} = -21\%$								
9	10673	I	335	6.18	3.55	−0.33	−0.19	110–165	110–165
	22.09.2004	V	335	5.78	6.14	−0.31	−0.33	110–165	110–165
	$\mathcal{P}^{\max}_{\max} = -74\%$	$\mathcal{P}$	335	3.6	4.92	−0.26	−0.26	110–165	110–165
	$\mathcal{P}^{\max}_{\text{aver}} = -35\%$								
	$\mathcal{P}^{\max}_{\text{SSRT}} = -22\%$								

Table 4. (Continued)

No	Object	Signals	n	t_1	t_2	r_1	r_2	P_1	P_2
10	10673	I	348	3.04	0.85	−0.16	−0.05	32, 38, 80, 175	85, 115
	23.09.2004	V	348	4.06	3.99	−0.22	−0.21	85, 115	85, 115
	$\mathcal{P}^{\max}_{\max} = -77\%$	$\mathcal{P}$	348	4.42	2.35	0.23	−0.13	35, 70, 115	35, 70, 115
	$\mathcal{P}^{\max}_{\mathrm{aver}} = -38\%$								
	$\mathcal{P}^{\max}_{\mathrm{SSRT}} = -21\%$								
11	10743	I	287	0.62	0.44	−0.04	−0.03	30, 45, 95, 150	30, 70, 100
	15.03.2005	V	287	1.82	2.65	0.11	0.15	140	140
	$\mathcal{P}^{\max}_{\max} = -63\%$	$\mathcal{P}$	287	5.06	2.80	−0.29	−0.16	40, 95	40, 70, 95, 150
	$\mathcal{P}^{\max}_{\mathrm{aver}} = -25\%$								
	$\mathcal{P}^{\max}_{\mathrm{SSRT}} = -18\%$								
12	10904	I	318	1.26	4.10	0.08	0.23	55, 160	55, 160
	16.08.2006	V	318	3.18	5.28	−0.18	−0.29	55, 160	55, 160
	$\mathcal{P}^{\max}_{\max} = -91\%$	$\mathcal{P}$	318	2.56	7.81	0.143	−0.41	40, 55, 105	35, 55, 90
	$\mathcal{P}^{\max}_{\mathrm{aver}} = -78\%$								
	$\mathcal{P}^{\max}_{\mathrm{SSRT}} = -9\%$								
13	10953	I	249	3.02	5.04	0.19	0.31	40, 80	60, 80, 120
	28.04.2007	V	249	1.27	0.96	0.08	0.06	80	60, 122
	$\mathcal{P}^{\max}_{\max} = -62\%$	$\mathcal{P}$	249	3.48	5.14	−0.22	−0.32	40, 80	40, 80
	$\mathcal{P}^{\max}_{\mathrm{aver}} = -44\%$								
	$\mathcal{P}^{\max}_{\mathrm{SSRT}} = -9\%$								
14	10953	I	268	5.38	5.28	0.32	0.31	55, 65, 135	55, 65
	01.05.2007	V	268	7.91	7.6	−0.45	−0.44	30, 38, 140	38, 52, 135
	$\mathcal{P}^{\max}_{\max} = -82\%$	$\mathcal{P}$	268	7.41	9.56	0.43	−0.53	50, 135	55, 135
	$\mathcal{P}^{\max}_{\mathrm{aver}} = -55\%$								
	$\mathcal{P}^{\max}_{\mathrm{SSRT}} = -6\%$								
15	10953	I	324	6.64	5.11	0.36	0.28	22, 30, 35, 52, 80	55, 80, 160
	02.05.2007	V	324	6.93	4.37	0.37	0.24	25, 32, 55, 82, 162	55, 85, 160
	$\mathcal{P}^{\max}_{\max} = -58\%$	$\mathcal{P}$	324	7.55	2.97	0.40	0.17	25, 35, 42, 65, 162	55, 80, 165
	$\mathcal{P}^{\max}_{\mathrm{aver}} = -17\%$								
	$\mathcal{P}^{\max}_{\mathrm{SSRT}} = -12\%$								

* The first column contains the number of the data series. The second column shows the information about the sunspot: the AR NOAA number, the day of the observation, maximum absolute values of the degrees of circular polarisation (in %) calculated for the maximum values of the radio brightness, $\mathcal{P}_{\max}$ and for the values averaged over the sunspot, $\mathcal{P}_{\mathrm{aver}}$ for NoRH, and $\mathcal{P}_{\mathrm{SSRT}}$ for SSRT (see subsections 2.1–2.3); the superscript "max" denotes the maximum value over the whole data series. The third column shows the signals used in the cross-correlation study: the brightness temperature in intensity I and polarisation V and the degree of polarisation $\mathcal{P}$. The fourth column gives the number of counts in the compared data sets. The fifth and sixth columns give the values of Student's t-coefficient for the cross-correlation of the SSRT signal and the NoRH signals constructed by the maximum values in each image and by the average value, respectively. The seventh and eighth columns give the cross-correlation coefficient for the cross-correlation of the SSRT signal and the NoRH signals constructed by the maximum values in each image and by the average value, respectively. The ninth and tenth columns show the significant periods P_1 and P_2 (in minutes) found in both SSRT and NoRH signals constructed by the maximum values in each image and the average value, respectively.

of the radio emission, the intensity, polarisation and degree of circular polarisation, may show LQPO with different periods simultaneously.

5. Statistical analysis of the radio emission recorded with SSRT and NoRH during the overlap of their observational times showed that there are common, statistically significant LQPO at 17 and 5.7 GHz simultaneously.

6. For nine out of fifteen days of observations, detrended 17 GHz and 5.7 GHz signals showed significant correlations with each other, with the cross-correlation coefficient greater than 0.3 and Student's t-coefficient greater than 3.41. Moreover, for five days of observations, the cross-correlation coefficient is significant for both intensity and polarisation signals.

Thus, our results confirm that LQPO are a robust feature of sunspot evolution. The detection of the same or similar periods in the time series of $T_{\mathrm{b}}^{(\mathrm{I})}$, $T_{\mathrm{b}}^{(\mathrm{V})}$, and $\mathcal{P}$, recorded at different heights in the sunspot's magnetosphere, suggest a global nature of the oscillations. In particular, the oscillation may be present in the variation of the magnetic field of the sunspot. In this case the slow variation of the magnetic field can be explained by global eigen oscillations of sunspots (Kshevetskii & Solov'ev 2008; Solov'ev & Kirichek 2008, 2009).

The rather poor (but significant) correlation of the 17 GHz

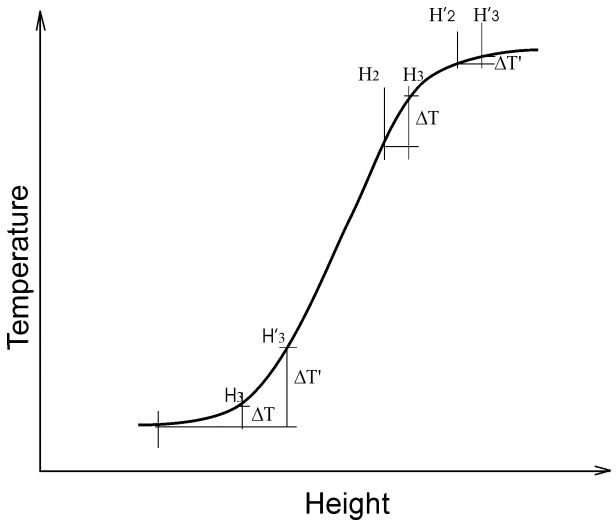

Fig. 8. Sketch of the location of emission levels at 17 GHz and 5.7 GHz above a sunspot. The solid curve shows the height variation of the temperature The vertical and horizontal lines show locations of the gyroresonance layers. The labels H2, H2′ and H3, H3′ show the heights of the 2nd and 3rd gyroresonance layers for two different instants of time that correspond to different phases of the oscillations of the magnetic field, respectively; the lower part of the curve refers to 17 GHz, the upper part of the curve refers to 5.7 GHz. ΔT and $\Delta T'$ are the temperature differences for two different instants of time.

and 5.7 GHz signals can be attributed to the difference in the emission formation heights and emission mechanisms, and to the specific state of the magnetosphere above the specific sunspot. Indeed, the source of the 17 GHz gyroresonance emission is situated at the height where the 3rd harmonics of the electron gyrofrequency is 17 GHz, while the 5.7 GHz emission comes from the regions where the 2nd and 3rd harmonics of the gyrofrequency are 5.7 GHz. Thus, the 5.7 GHz and 17 GHz signals may come from the regions that are significantly spatially separated.

Moreover, as is discussed in subsection 2.3 and shown in table 4 maximum values of the degrees of circular polarisation $\mathcal{P}^{\max}_{\max}$ and $\mathcal{P}^{\max}_{\rm aver}$ of the NoRH signals are in the range 50%–90%. Since this value is lower than 100%, it indicates that the observed emission contains a significant thermal bremstrahlung component in addition to the gyroresonance emission. On the other hand, the 5.7 GHz emission is fully gyroresonant (see, e.g., Zheleznyakov 1996). The low maximum degree of polarisation, 7%–22%, should be attributed to the simultaneous presence of the 2nd and 3rd harmonics of the gyrofrequency in the signal observed by SSRT, as well as to the geometrical and physical factors (e.g., the optical thickness of the source, electron temperature) . This may be an additional source of the de-correlation of the NoRH and SSRT signals.

The occasional anti-correlation of the 5.7 GHz and 17 GHz polarisation time series, evident in figure 7 and table 3, can be explained by the different sign of the temperature gradient at the heights of the 3rd gyro-layers for 17 GHz and 5.7 GHz frequencies. Figure 8 schematically shows the variation of the sunspot's temperature in the vertical direction and the heights of the gyroresonance layers for different frequencies. The gyroresonance layers are shown at different instants of time (and hence different heights) that correspond to different phases of the oscillations of the magnetic field. The 17 GHz signal comes from the lower layers of the sunspot's atmosphere, where the temperature curve has a positive sign of the second derivative, in contrast to the radiation at 5.7 GHz, where the sign of the second derivative is negative. For 17 GHz, the 2nd gyro layer is normally situated below the photosphere, and its emission does not reach the corona. The brightness temperature of extraordinary radiation is determined by the temperature of electrons at the 3rd gyro layer, while the brightness temperature of the ordinary radiation by the electron temperature at the 2nd gyro layer (Zheleznyakov 1996). Hence, the observed value of the signal in the polarisation channel is proportional to the difference of temperatures of the electrons at the heights of the 2nd and 3rd gyrolayer. Perturbations of the magnetic field, e.g., in an LQPO, changes the heights of the gyrolayers. In particular, an increase in the field causes an increase in the gyro-layer heights. In this case, the 5.7 GHz gyro-layers move to the regions with a lower gradient of the electron temperature, while the 17 GHz gyrolayer moves to the region of a higher electron temperature gradient (see figure 8). Thus, synphase oscillations of the magnetic field in the sunspot (e.g., in a global eigen oscillation of the sunspot) lead to the appearance of the same periodicity in the radio emission at all frequencies, in particular at 5.7 GHz and 17 GHz. However, the phase differences of the oscillations at 5.7 GHz and 17 GHz radiation can be anything from 0 to π. This effect may explain the observed phase differences. We conclude that the observed properties of LQPO are consistent with the global sunspot oscillation model developed in (Solov'ev & Kirichek 2008, 2009; Kshevetskii & Solov'ev 2008).

Two of the authors (IAB and VEA-M) are grateful to the LOC of the SPRO-2012 conference for the financial support. This work is supported by the Russian Foundation for Basic Research under grant number 13-02-00714, 13-02-00044, the Russian Ministry of Education and Science project No. 8524, the Marie Curie PIRSES-GA-2011-295272 *RadioSun* project, the European Research Council research project 321141 *SeismoSun* (VMN), and the Royal Society – Daiwa Anglo Japanese Foundation International Exchanges Scheme (VMN). Wavelet software was provided by C. Torrence and G. Compo.[2]

[2] Available at ⟨http://paos.colorado.edu/research/wavelets/⟩.

References

Abramov-Maximov, V. E., Gelfreikh, G. B., Efremov, V. I., Parfinenko, L. D., & Solovyev, A. A. 2007, in Proc. XI Pulkovo International Conference on Solar Physics, ed. A. V. Stepanov et al. (St.-Petersburg: Central Astronomical Observatory at Pulkovo), 3 (in Russian)

Aleshin, V. I., Kobrin, M. M., & Korshunov, A. I. 1973, Radiophys. Quantum Electron., 16, 571.

Bakunina, I. A., Abramov-Maximov, V. E., Lesovoy, S. V., Shibasaki, K., Solov'ev, A. A., & Tikhomirov, Yu. V. 2009, in IAU Symp., 257, Universal Heliophysical Processes, ed. N. Gopalswamy & D. F. Webb (Cambridge: Cambridge University Press), 155

Chorley, N., Hnat, B., Nakariakov, V. M., Inglis, A. R., & Bakunina, I. A. 2010, A&A, 513, A27

Chorley, N., Foullon, C., Hnat, B., Nakariakov, V. M., & Shibasaki, K. 2011, A&A, 529, A123

Durasova, M. S., Kobrin, M. M., & Yudin, O. I. 1971, Nature, 229, 82

Durasova, M. S., Lavrinov, G. A., Chandaev, A. K., & Yudin, O. I. 1968, Radiophys. Quantum Electron., 11, 993

Efremov, V. I., Parfinenko, L. D., & Solov'ev, A. A. 2007, Astron. Rep., 51, 401

Efremov, V. I., Parfinenko, L. D., & Solov'ev, A. A. 2008, J. Opt. Technol., 75, 144

Fuller, W. A. 1976, Introduction to Statistical Time Series (New York: Wiley), 366

Gelfreikh, G. B., Derevjanko, O. G., Korzhavin, A. N., & Stasjuk, N. P. 1969, Byull. Soln. Danny Acad. Nauk USSR, 9, 88

Gelfreikh, G. B., Nagovitsyn, Yu. A., & Nagovitsyna, E. Yu. 2006, PASJ, 58, 29

Kobrin, M. M., Pakhomov, V. V., Durasova, M. S., Timofeev, B. V., Prokof'eva, N. A., Lebedev, E. I., & Lavrinov, G. A. 1973, Radiophys. Quantum Electron., 16, 1036

Kosovichev, A. G. 2006, Adv. Space Res., 38, 876

Kshevetskii, S. P., & Solov'ev, A. A. 2008, Astron. Rep., 52, 772

Nagovitsyn, Yu. A., Nagovitsyna, E. Yu., & Abramov-Maximov, V. E. 2013, Astron. Rep., 57, 636

Nagovitsyn, Yu. A., & Vyal'Shin, G. F. 1990, Byull. Soln. Danny Acad. Nauk USSR, 9, 91

Nagovitsyna, E. Yu., & Nagovitsyn, Yu. A. 2002, Astron. Lett., 28, 121

Nakajima, H., et al. 1994, Proc. IEEE, 82, 705

Scargle, J. D. 1982, ApJ, 263, 835

Smirnova, V., Efremov, V. I., Parfinenko, L. D., Riehokainen, A., & Solov'ev, A. A. 2013a, A&A, 554, A121

Smirnova, V., Riehokainen, A., Ryzhov, V., Zhiltsov, A., & Kallunki, J. 2011, A&A, 534, A137

Smirnova, V., Riehokainen, A., Solov'ev, A., Kallunki, J., Zhiltsov, A., & Ryzhou, V. 2013b, A&A, 552, A23

Solov'ev, A. A. 1984a, Byull. Soln. Danny Acad. Nauk USSR, 1, 73

Solov'ev, A. A. 1984b, Soviet Astron., 28, 447

Solov'ev, A. A., & Kirichek, E. A. 2008, Astrophys. Bull., 63, 169

Solov'ev, A. A., & Kirichek, E. A. 2009, Astron. Rep., 53, 675

Sych, R. A., & Nakariakov, V. M. 2008, Sol. Phys., 248, 395

Torrence, C. & Compo, G. P. 1998, Bull. Am. Meteo. Soc., 79, 61

Torrence, C., & Webster, P. J. 1999, J. Climate, 12, 2679

Walpole, R., Myers, R., & Ye, K. 2002, Probability and Statistics for Engineers and Scientists, 7th ed. (Upper Saddle River, NJ: Pearson), 237

Yuan, D., Nakariakov, V. M., Chorley, N., & Foullon, C. 2011, A&A, 533, A116

Yudin, O. I. 1968b, Radiophys. Quantum Electron., 11, 342

Yudin, O. I. 1968a, Soviet Phys. Doklady, 13, 503

Zhao, J., & Kosovichev, A. G. 2004, ApJ, 603, 776

Zhao, J., Kosovichev, A. G., & Duvall, T. L. 2001, ApJ, 557, 384

Zheleznyakov, V. V. 1996, Radiation in Astrophysical Plasmas (Berlin: Springer)